

REVIEWS

Adv Clin Exp Med 2012, 21, 6, 831–841
ISSN 1899–5276

© Copyright by Wrocław Medical University

TOMASZ KRAŚNICKI^{A–D}, PRZEMYSŁAW PODGÓRSKI^{B, D, F}, MACIEJ GUZIŃSKI^{B, E},
ANNA CZARNECKA^B, KRZYSZTOF TUPIKOWSKI^{B, E}, JERZY GARCAREK^E, MAREK SĄSIADK^{A, E, F}

Novel Clinical Applications of Dual Energy Computed Tomography

Zastosowanie kliniczne dwuenergetycznej tomografii komputerowej

Department of General Radiology and Interventional Radiology and Neuroradiology, Wrocław Medical University, Poland

A – research concept and design; B – collection and/or assembly of data; C – data analysis and interpretation; D – writing the article; E – critical revision of the article; F – final approval of article; G – other

Abstract

Dual energy CT (DECT) was conceived at the very beginning of the computed tomography era. However the first DECT scanner was developed in 2006. Nowadays there are three different types of DECT available: dual-source CT with 80(100) kVp and 140 kVp tubes (Siemens Medical Solution); dual-layer multi-detector scanner with acquisition 120 or 140 kVp (Philips Healthcare); CT unit with one rapid kVp switching source and new detector based on gemstone scintillator materials (GE Healthcare). This article describes the physical background and principles of DECT imaging as well as applications of this innovative method in routine clinical practice (renal stone differentiation, pulmonary perfusion, neuroradiology and metallic implant imaging). The particular applications are illustrated by cases from author's material (*Adv Clin Exp Med* 2012, 21, 6, 831–841).

Key words: Dual Energy Computed Tomography, DECT, Computed Tomography, renal stones, pulmonary perfusion, metal implant imaging, neuroradiology.

Streszczenie

Podstawy fizyczne dwuenergetycznej tomografii były znane od początku istnienia tomografii komputerowej, jednak pierwsze tomografy dwuenergetyczne powstały dopiero w 2006 r. Obecnie do zastosowań klinicznych są dostępne 3 różne rodzaje tomografów dwuenergetycznych: tomograf dwulampowy (Siemens Medical Solution), aparat wielorzędowy o dwóch warstwach detektorów (Philips Healthcare) oraz tomograf jednoźródłowy z możliwością szybkiego przełączania napięcia na lampie rentgenowskiej (GE Healthcare). W tym artykule zostaną przedstawione fizyczne podstawy i zasady działania dwuenergetycznej tomografii komputerowej oraz kliniczne zastosowanie tej innowacyjnej metody obrazowania (w urologii, kardiologii, neuroradiologii i ortopedii). Poszczególne aplikacje zostały zilustrowane własnymi przykładami (*Adv Clin Exp Med* 2012, 21, 6, 831–841).

Słowa kluczowe: dwuenergetyczna tomografia komputerowa, DECT, tomografia komputerowa, kamienie nerkowe, perfuzja płucna, obrazowanie implantu metalowego, neuroradiologia.

The idea of computed tomography began with the mathematical basis proposed by Johann Radon in 1917. He created a mathematical tool, Radon Transform, which has been widely applicable to image reconstruction in computed tomography. In the late 1960's, Sir Godfrey Hounsfield and Allan Cormack invented the first CT scanner and developed it for commercial use. Since then, computed tomography has evolved from simple 1st genera-

tion CT to sophisticated ultra-fast multi-row detector CT with helical tube movement [1, 2].

The concept of multi-energy computed tomography has been known from the beginning of the CT era. [3] However technical difficulties only made it possible a few years ago to construct devices capable of generating two X-ray beams of low and high energy with a short time distance. Currently there are three technical approaches for dual energy CT.

Since 2006, many clinical applications of dual energy CT have been proposed [4] however the clinical usefulness of this method has not been established yet.

The purpose of this work is to present dual energy computed tomography principles, to discuss its clinical applications and consider the future perspectives of this technique.

The Physical and Technical Principles of Dual Energy Computed Tomography

Physical Background

X-ray is a form of electromagnetic radiation with a wavelength range from 0.01 to 10 nm, corresponding to frequencies in the range 10^{17} to 10^{18} Hz. X-rays with an energy range from 0.12 to 12 keV are called “soft” and with energy between 12 keV and 150 keV are called “hard”. For clinical purposes the most useful photon energy range is over 12 keV (“hard” X-rays) due to the penetrating abilities [5].

The main parameter responsible for X-ray imaging is the linear attenuation coefficient. In general, the linear attenuation coefficient is the measure of the changes of the X-ray beam intensity caused by the patient’s tissues.

The formula of X-ray intensity transmitted through the material (the patient’s tissues) is given by equation (1):

$$I = I_0 \exp(-\mu x) \quad (1)$$

Where I is the transmitted X-ray intensity, I_0 is the initial intensity of the X-ray beam, μ is the linear attenuation coefficient (cm^{-1}), x is the material thickness [6, 7].

The linear coefficient reflects the removal of photons from a beam by interaction with material electrons. These interactions are photon absorption (photoelectric effect) and/or scattering (Compton Effect). The mass attenuation coefficient is approximately constant for different materials in a specified energy range, hence it is strongly determined by the material density.

Dual Energy Computed Tomography

Dual Energy Computed Tomography (DECT) is a medical imaging method which uses two data sets from the same anatomic location with different kVp (usually 80/100 and 140 kVp) [8, 9].

There are three different commercially available concepts of Dual Energy CT (DECT) with three different ways of providing simultaneous acquisition of data during a single examination.

The first concept, which was developed by Siemens Medical Solutions, is based on the technology of two X-ray tubes (dual source imaging) working simultaneously in 64 or 128-row detector scanners (Somatom Definition and Somatom Definition Flash) with 0.625/1 mm collimation. The tubes may work with two modes, 140/80 kVp and 140/100 kVp, and are arranged at right angles to each other which implicates a small FOV (field of view), 26 cm with Siemens SOMATOM Definition, and a larger FOV, 33 cm with SOMATOM Definition Flash [4, 7] (Fig. 1 a, b).

The second method, proposed by Philips Healthcare, is based on the use of a dual-layer multi-detector (sandwich layer) scanner configuration (Brilliance 64) with one X-ray tube performing acquisition at high energy (e.g. 120 or 140 keV). The detector has two “sandwich” layers – the top layer absorbs most of the low-energy spectrum (approximately 50% of the beam), while the bottom detector layer absorbs higher energy photons. Images are reconstructed separately from the data of the top and bottom layers. There is no need to provide separated low and high energy beams. The Philips Dual layer CT unit uses a 32 slice dual-layer scanner with 64 electronic channels (2 per each dual-layer detector element), slice thickness 0.625/1 mm and field of view = 50 cm (Fig. 2).

The third concept, developed by GE Healthcare, is based on the use of one X-ray tube with “fast kV-switching” (about 0.4 ms time interval) between 80 kVp and 140 kVp energies and a new generation of 64-row gemstone detectors with a slice thickness 0.625/1.25 mm (Fig. 3)

The technical principles of the most important parameters of the dual-energy systems mentioned above are presented in Table 1.

The data obtained from any DECT scanner can be evaluated with a dedicated workstation using special software.

DECT Principles

The main principle of dual energy CT is material decomposition based on different attenuation coefficients which depends on the energy levels of the X-ray beam (Fig. 4). It enables better assessment of materials and images without the beam hardening effects during reconstruction at the selected monochromatic energy. It gives also information about effective atomic number and mass density maps, in the form of basic materials e.g. water or

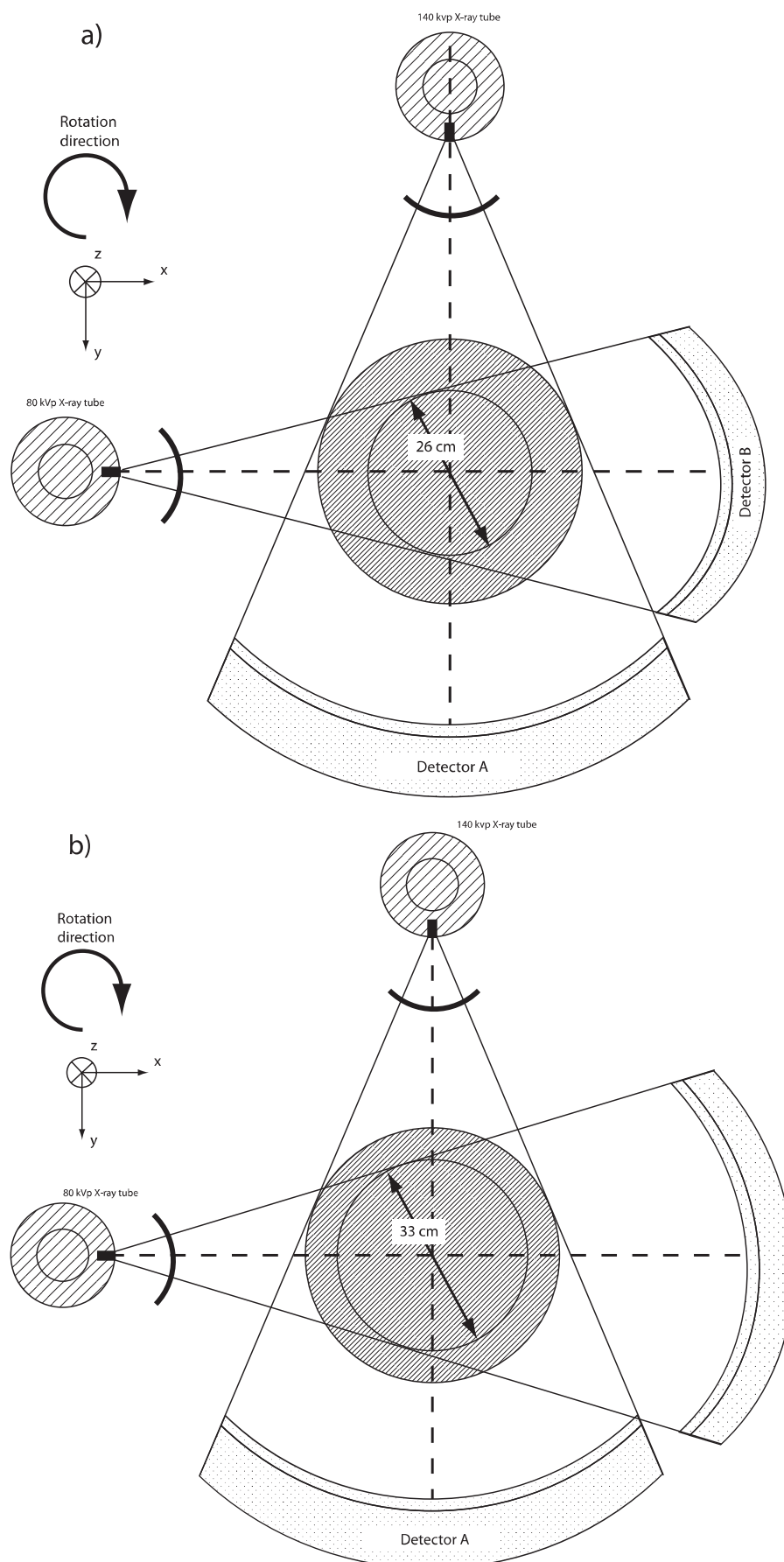


Fig. 1. Schematic drawings of the SIEMENS Dual Energy CT scanners: a) SOMATOM Definition; b) SOMATOM Definition Flash [4]

Ryc. 1. Schemat urządzenia SIEMENS Dual Energy CT: a) SOMATOM Definition; b) SOMATOM Definition Flash [4]

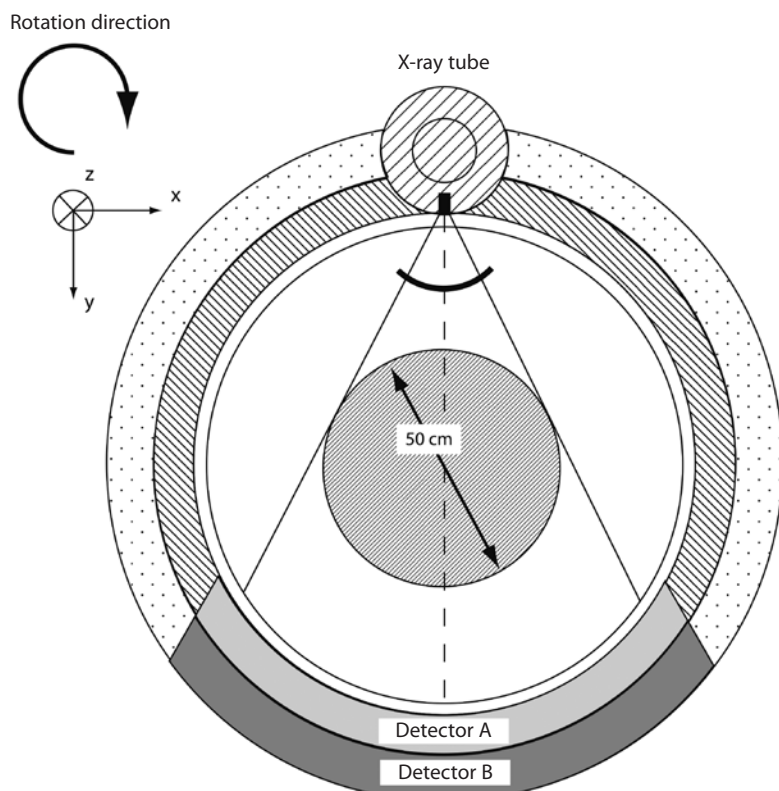


Fig. 2. Schematic drawing of PHILIPS Healthcare Dual Energy CT scanner: modified Brilliance 64 CT [4]

Ryc. 2. Schemat urządzenia PHILIPS Healthcare Dual Energy CT: zmodyfikowany Brilliance 64 CT [4]

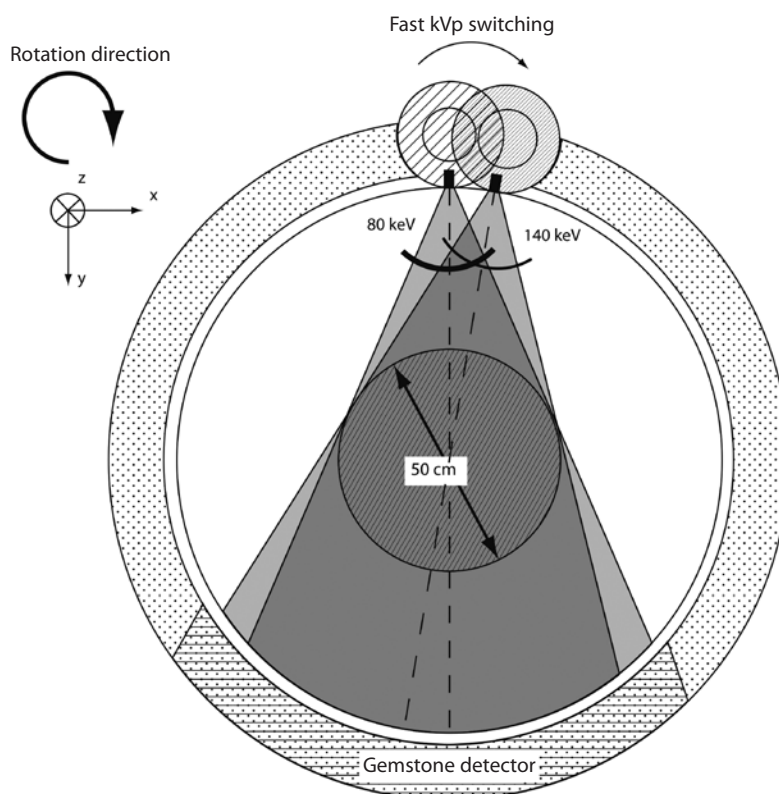


Fig. 3. Schematic drawing of GE Healthcare Dual Energy CT scanner: Discovery 750HD

Ryc. 3. Schemat urządzenia GE Healthcare CT: Discovery 750HD

calcium. These materials' density suppresses one basic material and enhances the other.

X-ray Tube

An X-ray tube is a vacuum tube with a cathode and rotating anode disc inside. The X-ray

beam is produced during collisions of electrons emitted from the cathode to the anode material. Electrons are accelerated in the X-ray tube as a result of the difference of potential between the cathode and anode. The X-ray spectrum depends on the anode material (tungsten, molybdenum or copper alloy) and the voltage. In

Table 1. Technical principles of DECT systems [9]

Tabela 1. Zasady techniczne systemów DECT [9]

Specific features	64-slice dual source MDCT (Definition)	128-slice dual source MDCT (Definition Flash)	64-Channel MDCT (Brilliance 64)	64-MDCT (Discovery 750HD)
Detector configuration	2×32×0.625	2×64×0.625	2×32×0.625	64×0.625
Slice thickness [mm]	0.6/1.2	0.6/1.2	0.625/1	0.625/1.25
Field of view (FOV) [cm]	26	33	50	50
Time interval between images [ms]	83	75	–	0.3–0.5
Techniques used for dual energy	2 tubes	2 tubes	dual layer detectors	fast kVp switching
Gantry rotation time for dual-energy acquisition [ms]	330	300	400	350
Temporal resolution for dual-energy acquisition [ms]	165	150	–	175

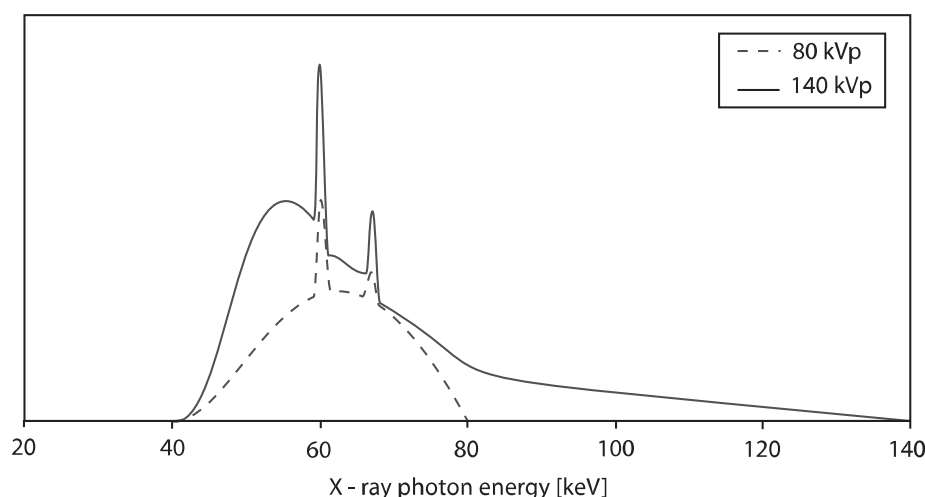


Fig. 4. X-ray spectra used in dual energy decomposition

Ryc. 4. Widmo rentgenowskie stosowane w podwójnym rozkładzie energii

CT units, the tube voltage ranges from 80 to 150 kVp [2, 5].

Using of two different energies for DECT examination brings two sets of image data and makes it possible to avoid misregistration as well as to reduce beam hardening artifacts. Images obtained at 80 kVp have a higher image contrast factor than at 140 kVp. Hounsfield unit measurements are not absolute and are dependent on the kVp used for acquisition.

It is important to have the gap between the spectra in tube/tubes used for dual-energy CT acquisitions as low as possible. A tube voltage lower than 80 kVp is not recommended because of the photon absorption properties of the human body. On the other hand, values exceeding 140 kVp may result in very low soft tissue contrast.

In this diagnostic range of energy between 80 and 140 kVp, the attenuation coefficient for a given material can be described as a linear combination of Compton scattering and the photoelectric effect [2, 7]:

$$\mu(x, y, z, E) = a_c(x, y, z)f_{KN}(E) + a_p(x, y, z)f_p(E) \tag{2}$$

where (x,y,z) are location coordinates of the material, $\mu(x, y, z, E)$ is the total X-ray attenuation, E is the incident energy, $f_p(E)$ approximates the energy dependence on the photoelectric interactions dependent on electron density. $f_{KN}(E)$ is the Klein-Nishina cross section for Compton effects [7, 11]

It can be more simply described as:

$$\mu(x, y, z, E) = \mu_{compton}(E) + \mu_{photoelectric}(E) \tag{3}$$

CT images are performed using Hounsfield units, thus the Hounsfield unit value can be calculated from the attenuation coefficient:

$$HU = 1000 \times \frac{\hat{\mu} - \hat{\mu}_{water}}{\hat{\mu}_{water}} \tag{4}$$

where $\hat{\mu}_{water}$ is the average water attenuation coefficient [4, 7].

Rapid Voltage Switching

There are two ways of providing exposure in DECT: using two X-ray sources with high and low energy beams and using one source with fast kV switching. The GE Discovery 750HD CT unit which is used in our department has one X-ray tube with fast kVp switching. The interval for switching between 80 and 140 kVp in this unit is about 0.4 ms. This solution has the major advantage of decreased cost, because there is no need to equip the unit with additional hardware. The disadvantage of this technology is a non-rectangular voltage retention on the X-ray tube with limited adaptation of the current, which leads to a much lower signal at low energy than at high energy.

Gemstone Detector

In DECT technology, it is necessary to use a detector which may differentiate quantities of different energies, provides angular view sampling within the constraints of medical diagnostic rotation speeds and is capable of detecting rapid kV fluctuation. GE Healthcare solved this problem using gemstone scintillator materials. It is a complex of crystalline structure material based on rare earth oxide. It allows for imaging with high light output, fast primary speed with very low afterglow [4], and undetectable radiation damage. Slice thickness of these detectors is about 0.625 mm. The gemstone has a very low decay time (30 ns), which is 100 times lower than a conventional Gd_2O_2S scintillator and a much lower level of afterglow (25% of the Gd_2O_2S scintillator's afterglow). The gemstone scintillator is also compatible with a fast sampling capability data acquisition system, which enables simultaneous acquisition of low and high kVp sinograms at customary rotation speed and thus contributes to a minimization of the patient's radiation dose. [4]

Image Reconstruction

Following the acquisition, calibration of the data is applied. Because of non-ideal kVp fluctuation during the examination, it is hard to find a fixed kVp of the same spectral response because of the real fast kVp switching energy spectrum. The overall spectrum is decomposed as a superposition of known kVp spectra:

$$S_p(E) = \sum_k^{N_k} \alpha_k S_k(E) \quad (5)$$

Where $S_k(E)$ are basis spectra (of total N_k number) of the fixed kVp, α_k are weights coefficients of the basis spectra. Response to this spectrum self-normalized detector can be described by the equation (5):

$$R(d) = \frac{\sum_k \alpha_k G_k(d)}{\sum_d \sum_k \alpha_k G_k(d)} \quad (6)$$

The value of $R(d)$ can be measured using a fast switching air scan, $G_k(d)$ is based on the system geometry calculation. The α_k value needs to be found by solving the equation.

Calibration corrections have been applied to the data of low and high kVp sets. The signal from the non-ideal kVp rise/fall is aligned in projection space. The next step is to transform the images into a projection of basis pair materials (e.g. water and iodine) [4]. This tool provides iodine maps that have the potential to determine contrast enhancement or iodine separation from the anatomic background.

Two energy acquisitions make it possible to create a virtual extrapolated energy range from 40 to 140 keV which can be useful to identify low-contrast lesions.

Clinical Application

The clinical images presented in this article were acquired by a 64-Multi Detector CT (MDCT) unit (Discovery 750HD, GE Healthcare). All data acquired from the GSI urinary stones DECT protocol were postprocessed on a ADW 4.5 workstation (GE Healthcare).

Urinary Applications

The main issue in patients with urolithiasis is the proper choice of a treatment method, including invasive procedures with may lead to complications. There is no doubt that the knowledge of urinary stone chemical components may influence the method of treatment and make it possible to avoid invasive procedures in many cases.

Dual Energy Computed Tomography gives a powerful tool which can be a milestone in urinary stone treatment. Using two different X-ray beam energies to the same material, it is possible to calculate the effective atomic number (Z_{eff}) of this material. Attenuation coefficient is very dependent on the effective atomic number of the material and

the energy of the X-rays interacting with the material. Light chemical elements (such as H, C, N, O) have smaller Z_{eff} value and absorb X-rays in a dif-

ferent way than heavier elements (P, Ca, S, I). Z_{eff} is the effective atomic number of the mixture or compound and the formula for Z_{eff} is as below:

$$Z_{\text{eff}} = \sqrt[\alpha]{f_1 \times (Z_1)^\alpha + f_2 \times (Z_2)^\alpha + f_3 \times (Z_3)^\alpha + \dots + f_n \times (Z_n)^\alpha} = \sqrt[\alpha]{\sum_{i=1}^n f_i \times (Z_i)^\alpha} \quad (7)$$

Where f_i is the fraction of the total number of electrons associated with particular elements, and Z_i is the atomic number of particular elements. The exponent α is not a constant but dependent on the photon energy and can have values between 2 and 4 [3, 4].

According to the equation (5) it is possible to estimate the theoretical value of Z_{eff} for each of the common urinary stones, however there are variations of Z_{eff} values obtained by the equation (7), dependent on the α factor. For common urinary stone types, Z_{eff} was calculated with two different α factor values (Table 2):

Case

A 60-year-old male patient was examined using DECT Discovery 750HD with GSI (Gemstone Spectral Imaging) protocol "Renal Stones". Effective atomic number analysis by GE Healthcare software demonstrated that in vivo renal stone examination Z_{eff} value was 13.75 (+/- 0.2) (Fig. 5).

After surgical removal of the renal stone, an *in vitro* study of the same stone showed Z_{eff} value = 13.9 (+/- 0.2) (Fig. 6). These results correspond to the theoretically calculated Z_{eff} of the calcium oxalate stone (Table 2).

Chemical analysis of the stone material confirmed that it was composed of 100% calcium oxalate.

Cardiopulmonary Applications

Dual-energy CT provides a unique method of pulmonary embolism assessment. Using GSI Z_{eff} maps or generated iodine maps for lung perfusion, it can detect both tiny thrombus or embolus inside the pulmonary artery and a perfusion defect in the affected lung tissue.

Case

A 60-year-old female patient with dyspnea and suspicion of pulmonary embolism was referred to

Table 2. Common urinary stone types

Tabela 2. Typowe rodzaje kamieni nerkowych

Urinary stones (chemical formula)	Chemical formula	Z_{eff} ($\alpha=3.9$)	Z_{eff} ($\alpha=2.94$)
Uric acid	$C_5H_4N_4O_3$	6.98	6.91
Uric acid dihydrate	$C_5H_4N_4O_3 \cdot 2H_2O$	7.10	7.01
Ammonium urate	$C_5H_3N_4O_3 \cdot NH_4$	6.92	6.84
Calcium oxalate monohydrate	$CaC_2O_4 \cdot H_2O$	14.52	13.45
Calcium oxalate dihydrate	$CaC_2O_4 \cdot 2H_2O$	14.09	12.99
Calcium hydroxyapatite	$Ca_{10}(PO_4)_6(OH)_2$	16.36	15.86
Carbonate apatite	$Ca_{10}(PO_4)_6(CO_3)_2(OH,CO_3)_2$	14.98	15.40
Calcium phosphate	$Ca_3(PO_4)_2$	16.38	15.81
Brushite	$CaHPO_4 \cdot 2H_2O$	14.66	13.82
Struvite	$MgNH_4PO_4 \cdot 6H_2O$	10.13	10.23
Cystine	$C_6H_{12}N_2O_4S_2$	11.60	10.78

Effective atomic number of all types of stones is similar for $\alpha = 2.94$ and $\alpha = 3.9$.

Dual energy data can be used to characterize urinary stones. The results obtained are reliable and accurate to theoretically calculated Z_{eff} .

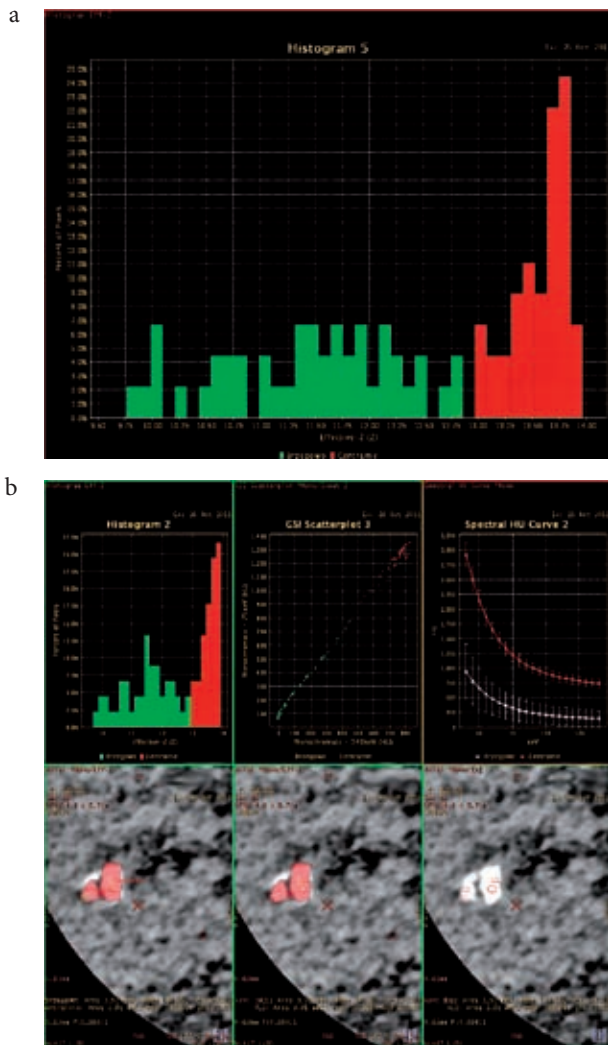


Fig. 5. Renal stone *in vivo* images of 60-year-old patient: (a) Z_{eff} histogram of renal stone, red histogram shows Z_{eff} from centrally located Region of Interest (ROI) in the stone, green histogram reveals the border part of the calculus; (b) Axial DECT image obtained by dual energy CT. ROI analyses are presented on the histogram, scatterplot and spectral HU curve plots. Department of General and Interventional Radiology and Neuroradiology Wrocław Medical University, 2012

Ryc. 5. Kamień nerkowy *in vivo* u 60-letniego pacjenta: (a) histogram Z_{eff} kamienia nerkowego, czerwony histogram pokazuje Z_{eff} z centralnie położonego obszaru zainteresowania (ROI) w kamieniu, zielony histogram ukazuje graniczną część kamienia; (b) osiowy obraz DECT uzyskany za pomocą dwuenergetycznej TK. Analiza ROI jest pokazana na histogramie, wykresie rozrzutu i spektralnej krzywej HU. Zakład Radiologii Ogólnej, Zabiegowej i Neuroradiologii, Uniwersytet Medyczny we Wrocławiu, 2012

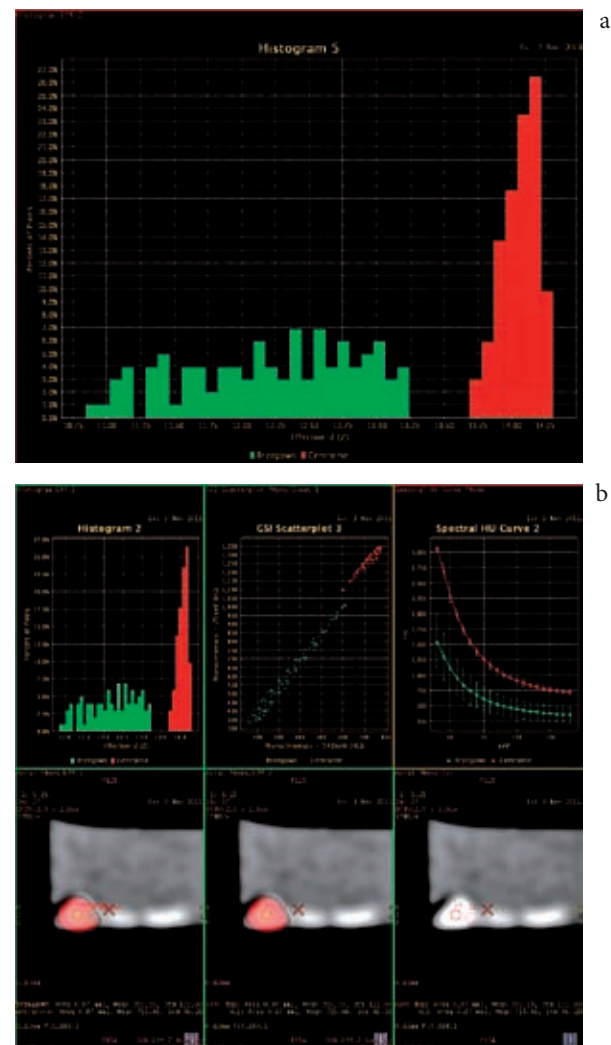


Fig. 6. Renal stone *in vitro* images of the same patient: (a) Z_{eff} histogram of renal stone, red histogram shows Z_{eff} from central arranged Region of Interest (ROI) in the stone, green histogram reveals the border part of calculus; (b) Axial DECT image obtained by dual energy CT. ROI analyses are presented on the histogram, scatterplot and spectral HU curve plots. Department of General, Interventional Radiology and Neuroradiology Wrocław Medical University, 2012

Ryc. 6. Kamień nerkowy w obrazach *in vitro* u tego samego pacjenta: (a) histogram Z_{eff} kamienia nerkowego, czerwony histogram pokazuje Z_{eff} z centralnie położonego obszaru zainteresowania (ROI) w kamieniu, zielony histogram ukazuje graniczną część kamienia; (b) osiowy obraz DECT uzyskany za pomocą dwuenergetycznej TK. Analiza ROI jest pokazana na histogramie, wykresie rozrzutu i spektralnej krzywej HU. Zakład Radiologii Ogólnej, Zabiegowej i Neuroradiologii, Uniwersytet Medyczny we Wrocławiu, 2012

the urgent CTA of pulmonary arteries. Examination showed thrombi in the main pulmonary arteries. Advanced GSI Z_{eff} assessment revealed a lung perfusion defect in the 10th segment of the

left lung. A spectral HU curve diagram confirmed a significant difference between the ROI from normal lung tissue and ROI from the suspicious area (Fig. 7).

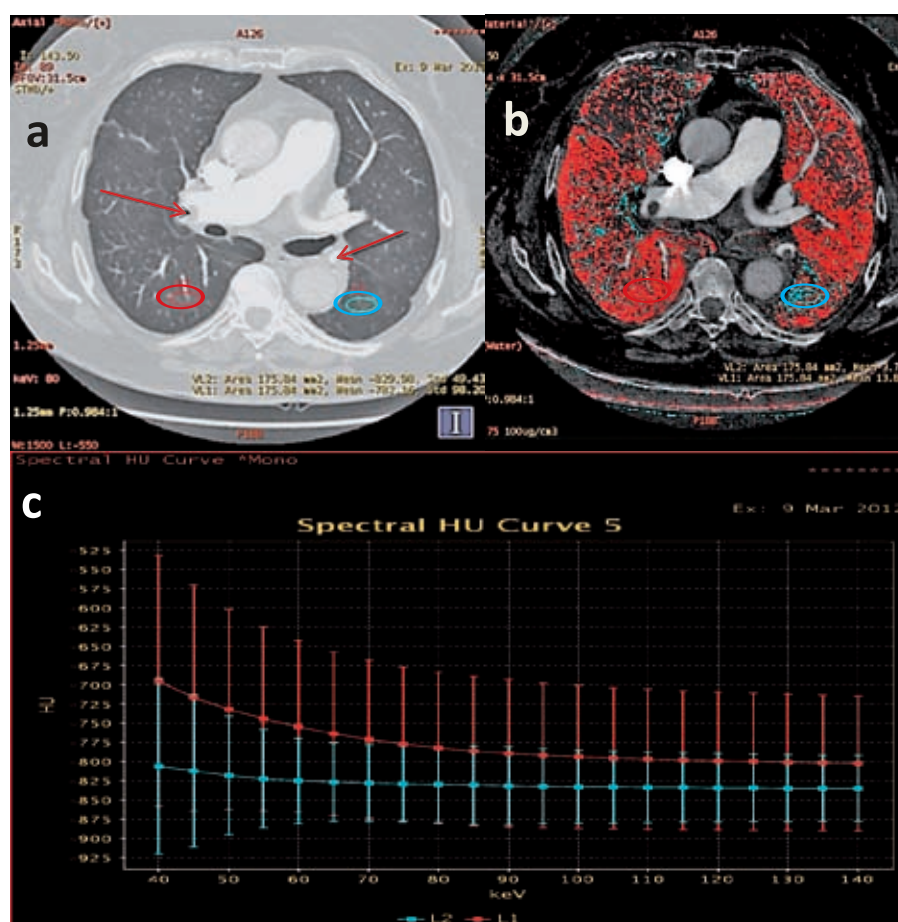


Fig. 7. Axial chest images: a) thrombi in left and right pulmonary arteries (arrows), GSI ROI localization (open arrows), b) Color Z_{eff} map of pulmonary embolism. Red color – normal perfusion, blue color with focal lung perfusion defect in the 10th segment of the left lung. c) Spectral HU curve diagram from ROIs. Department of General Radiology, Interventional Radiology and Neuroradiology Wrocław Medical University, 2012

Ryc. 7. Osiowe zdjęcie klatki piersiowej: a) skrzepliny w lewej i prawej tętnicy płucnej (strzałki), umieszczenie GSI ROI (otwarte strzałki); b) kolorowa mapa Z_{eff} zatorowości płucnej. Kolor czerwony – prawidłowa perfuzja, kolor niebieski – ogniskowe uszkodzenie perfuzji płuc w 10. segmencie płuca lewego; c) spektralna krzywa HU z ROI. Zakład Radiologii Ogólnej, Zabiegowej i Neuroradiologii, Uniwersytet Medyczny we Wrocławiu, 2012

Metal Artifact Reduction Applications

The main problem with imaging metallic objects is the presence of artifacts which results in difficulties in the assessment of surrounding bones and tissues. The metal artifacts are caused by photon starvation and beam hardening. Due to photon starvation, the number of photons which pass through the metallic object is less than the number of photons passing through non-metallic objects. It causes much a lower signal-to-noise ratio (SNR) in the measured projection data compared to non-metallic artifact images [12]. On the other hand, in the beam hardening phenomenon, the X-Ray beam with lower energy is much more absorbed than the beam with higher energy while penetrating an object, due to the high attenuation of the material. The remaining photons have higher energy and

better penetrating abilities. [13, 14] This issue can be solved by application of the specific algorithms such as linear interpolation of reprojected metal traces and multi-dimensional adaptive filtering of the raw data. DECT technology, which makes it possible to obtain spectral information concerning different data sets depending on the beam energy level, can provide a significant reduction of artifacts from metal objects. DECT Metal Artifacts Reduction algorithms are very helpful in the assessment of prostheses and other metal implants, and can provide important information, e.g. the presence of fractures or loosening, precise visualization of the implants' coverage and ruling out hematoma or inflammation in the adjacent soft tissues [13, 15].

Case

A 58-year-old male patient with stabilization of pelvis fracture with metal screws and suspicion

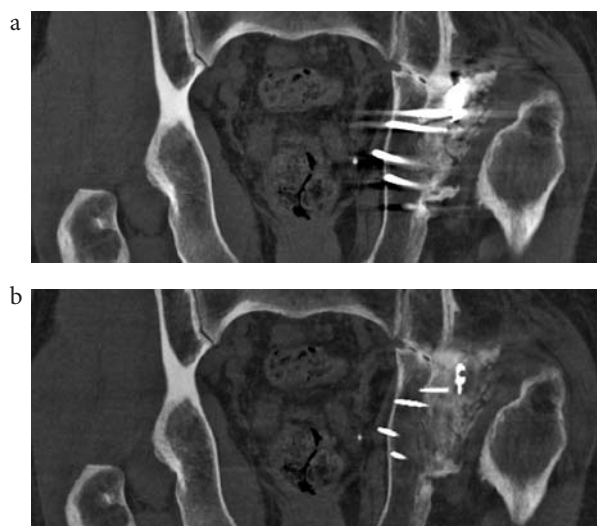


Fig. 8. Coronal image of pelvis with metal implants a) without GSI MARS algorithm; b) with GSI MARS algorithm. Marked reduction of artifacts after application of the MARS algorithm. Department of General, Interventional Radiology and Neuroradiology Wrocław Medical University, 2012

Ryc. 8. Obraz miednicy z metalowymi implantami w płaszczyźnie czołowej a) bez GSI algorytmu MARS; b) z GSI algorytmem MARS. Znaczne ograniczenie artefaktów po zastosowaniu algorytmu MARS. Zakład Radiologii Ogólnej, Zabiegowej i Neuroradiologii, Uniwersytet Medyczny we Wrocławiu, 2012

of bone damage was examined using DECT Discovery 750HD with GSI (Gemstone Spectral Imaging) using a Metal Artifact Reduction (MARS) protocol (GE Healthcare). After application of the MARS algorithm, we obtained images with a significant reduction of metallic artifacts (Fig. 8) thus it was possible to evaluate bone lesions. The MARS algorithm seems to be very useful in precise radiological assessment of the bone structures in patients with metal implants.

Neuroradiology Applications

The region of the intracranial space adjacent to the skull base, e.g. the suprasellar area, is hard to evaluate in a CT examination due to beam hardening artifacts. Dual energy CT eliminates those artifacts and makes this region easy to evaluate. The beam hardening artifacts are reduced significantly by GSI applications. It provides better visualization of anatomical and pathological structures hidden from the interpretation (Fig. 9).

Future Perspectives

Dual Energy CT provides new diagnostic possibilities, however it is still an innovating technique which needs clinical verification.

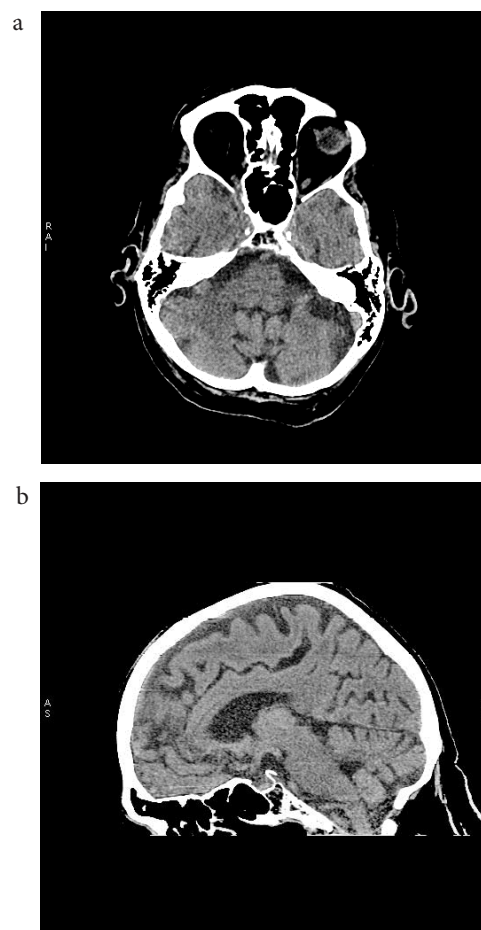


Fig. 9. Axial and sagittal CT brain images obtained with DECT: a) axial brain image, b) sagittal brain image. Good visualization of skull base regions, no artifacts visible. Department of General, Interventional Radiology and Neuroradiology Wrocław Medical University 2012

Ryc. 9. Osiove i strzałkowe obrazy TK mózgu uzyskane za pomocą DECT: a) osiowy obraz mózgu, b) strzałkowy obraz mózgu. Dobra wizualizacja podstawy czaszki, bez widocznych artefaktów. Zakład Radiologii Ogólnej, Zabiegowej i Neuroradiologii, Uniwersytet Medyczny we Wrocławiu, 2012

With a more precise detecting system such as photon counting detectors [16], evaluation of the DECT images, according to Z_{eff} measurements, can be a powerful tool for lesion assessment. The main challenge is to create new algorithms providing the creation of Z_{eff} tissue maps. This tool would be a great step toward X-ray CT tissue spectroscopy.

The main disadvantage of DECT is the increased examination dose resulting from the use of two X-ray energies.

On the other hand, there are several ways to reduce patient dose, beginning with currently available advanced reconstruction algorithms like iterative reconstruction (ASiR, MBIR) [17] to more

sensitive photon counting detectors, which will be available in the future. The model based iterative reconstruction algorithm seems to be the future of image reconstruction in CT and its application to DECT imaging which is currently unavailable for clinical use.

Conclusions

The major advantages of DECT is material decomposition based on the use of two different energies which provide two image series with different kVp and the elimination of misregistration and artifacts. This allows for precise assessment of images, which may provide better detection and identification of particular lesions in the body and tissue differentiation which can be applied to many fields in medicine.

References

- [1] **Hendrich B, Zimmer K, Guzinski M, Sasiadek M:** Application of 64-Detector Computed Tomography Myelography in the Diagnostics of the Spinal Canal. *Adv Clin Exp Med* 2011, 20, 3, 351–361.
- [2] **Duerk JL:** Principles of Computed Tomography and Magnetic resonance imaging. In: *CT and MR imaging of the whole body*. Eds.: Haaga JR, Lanzieri CF. 2003, 22–36. Mosby, St. Lois.
- [3] **Alvarez RE, Macovski A:** Energy-selective reconstruction in X-ray computerized tomography. *Phys Med Biol* 1976, 21, 733–744.
- [4] **Johnson TRC et al. (eds.):** Dual Energy CT in Clinical Practice. *Medical Radiology*, Springer-Verlag Berlin Heidelberg 2011.
- [5] **Seibert JA:** X-Ray Imaging Physics for Nuclear Medicine Technologists. Part 1: Basic Principles of X-Ray Production. *J Nucl Med Technol* 2004, 32 (3), 139–147.
- [6] **Schram RPC:** X-Ray Attenuation: Application of X-ray imaging for density analysis. NRG report 20002/01.44395/I, 2001.
- [7] **Haghighi RR, Chatterjee S, Vyas A, Kumar P, Thulkar S:** X-ray attenuation coefficient of mixtures: Inputs for dual-energy CT. *Med Phys* 2011, 38 (10), 5270–5279.
- [8] **Barett JF, Keat N:** Artifacts in CT: Recognition and Avoidance. *RadioGraphics* 2004, 24, 1679–1691.
- [9] **Karçaltıncaba M, Aktaş A:** Dual-energy CT revisited with multidetector CT: review of principles and clinical applications. *Diagn Interv Radiol* 2011, 17(3), 181–194.
- [10] **Zou Y, Silver MD:** Analysis of Fast kV-switching in Dual Energy CT using a Prereconstruction Decomposition Technique. *Medical Imaging 2008, Physics of Medical Imaging, Proc. of SPIE* 2008, 6913, 691313.
- [11] **Ying Z, Naidu R, Crawford CR:** Dual energy computed tomography for explosive detection. *J X-Ray Sci Technol* 2006, 14, 235–256.
- [12] **Jeong KY, Ra JB:** Reduction of artifacts due to multiple metallic objects in computed tomography. *Medical Imaging 2009: Physics of Medical Imaging Proc. of SPIE* 2009, 7258, 72583E.
- [13] **Lee YH, Park KK, Song HT, Kim S, Suh JS:** Metal artefact reduction in gemstone spectral imaging dual-energy CT with and without metal artefact reduction software. *Eur Radiol* 2012, Feb 4 [Epub ahead of print].
- [14] **Ramakrishna K, Muradlidhar K, Munshi P:** Beam hardening in simulated X-ray. *NDT E Int* 2006, 39, 449–457.
- [15] **Bamberg F, Dierks A, Nikolaou K, Reiser MF, Becker CR, Johnson TR:** Metal artifact reduction by dual energy computed tomography using monoenergetic extrapolation. *Eur Radiol* 2011, 21, 1424–1429.
- [16] **Shikhaliev PM, Fritz SG:** Photon counting spectral CT versus conventional CT: comparative evaluation for breast imaging application. *Phys Med Biol* 2011, 56, 1905.
- [17] **Yu Z, Thibault JB, Bouman CA, Sauer KD, Hsieh J:** Fast model-based X-ray CT reconstruction using spatially nonhomogeneous ICD optimization. *IEEE Trans Image Process* 2011, 20(1), 161–175.

Address for correspondence:

Tomasz Kraśnicki
Department of General Radiology and Interventional Radiology and Neuroradiology
University Hospital
Borowska 213
50-556 Wrocław
Poland
E-mail: tomasz.krasnicki@gmail.com

Conflict of interest: None declared

Received: 24.05.2012

Revised: 24.08.2012

Accepted: 12.12.2012